

# Live Avatar: Streaming Real-time Audio-Driven Avatar Generation with Infinite Length

Yubo Huang<sup>1,2</sup> Hailong Guo<sup>2,3</sup> Fangtai Wu<sup>2,4</sup> Shifeng Zhang<sup>2</sup> Shijie Huang<sup>2</sup>  
 Qijun Gan<sup>4</sup> Lin Liu<sup>1</sup> Sirui Zhao<sup>1,\*</sup> Enhong Chen<sup>1,\*</sup> Jiaming Liu<sup>2,†</sup> Steven Hoi<sup>2</sup>

<sup>1</sup> University of Science and Technology of China <sup>2</sup> Alibaba Group  
<sup>3</sup> Beijing University of Posts and Telecommunications <sup>4</sup> Zhejiang University

snake1124@mail.ustc.edu.cn  
 liujiaming.ljl@alibaba-inc.com

\* Corresponding authors.

† Project Leader.



Figure 1. We propose Live Avatar, a powerful real-time streaming model capable of infinitely long audio-driven avatar generation, producing lifelike avatars that talk, react, and persist seamlessly over hours.

## Abstract

Existing diffusion-based video generation methods are fundamentally constrained by sequential computation and long-horizon inconsistency, limiting their practical adoption in real-time, streaming audio-driven avatar synthesis. We present Live Avatar, an algorithm-system co-designed framework that enables efficient, high-fidelity, and infinite-length avatar generation using a 14-billion-parameter diffusion model. Our approach introduces Timestep-forcing Pipeline Parallelism (TPP), a distributed inference paradigm that pipelines denoising steps across multiple GPUs, effectively breaking the autoregressive bottleneck and ensuring stable, low-latency real-time streaming. To further enhance temporal consistency and mitigate identity drift and color artifacts, we propose the

*Rolling Sink Frame Mechanism (RSFM), which maintains sequence fidelity by dynamically recalibrating appearance using a cached reference image. Additionally, we leverage Self-Forcing Distribution Matching Distillation to facilitate causal, streamable adaptation of large-scale models without sacrificing visual quality. Live Avatar demonstrates state-of-the-art performance, reaching 20 FPS end-to-end generation on 5 H800 GPUs, and, to the best of our knowledge, is the first to achieve practical, real-time, high-fidelity avatar generation at this scale. Our work establishes a new paradigm for deploying advanced diffusion models in industrial long-form video synthesis applications.*

**Project page:** <https://liveavatar.github.io>

## 1. Introduction

Audio-driven avatar generation, the synthesis of photorealistic human face video conditioned solely on an input audio stream, is a foundational technology for interactive digital communication. Its applications are expansive, ranging from virtual reality and live streaming to digital assistants. The demand for systems capable of producing high-fidelity, expressive, and real-time avatars has driven significant recent advancements, particularly with the rise of diffusion models for high-fidelity video synthesis[2, 17, 40].

Despite their success in setting new benchmarks for visual quality, deploying these powerful generative models in real-time, streaming environments faces fundamental and conflicting challenges.

The first challenge is the real-time fidelity dilemma. Large-scale diffusion models[14] provide unmatched visual detail but suffer from high inference latency. Their inherent reliance on the sequential denoising computation leads to a latency profile that is fundamentally incompatible with interactive scenarios requiring low latency and high frame rates (e.g.,  $\geq 20$  FPS). The complex trade-off between model capacity, visual quality, and practical execution speed remains a critical bottleneck for deployment.

The second challenge is the long-horizon consistency. Applications demanding infinite-length or long-horizon generation necessitate continuous temporal stability. Existing methodologies are highly susceptible to limited expression or the gradual accumulation of identity drift and distracting color artifacts over prolonged synthesis periods as revealed in some works[20, 38], severely compromising the avatar’s coherence and the viewer’s experience.

To address these critical challenges, we propose **Live Avatar**, a novel training and inference framework. Live Avatar is designed to fundamentally enable large diffusion models (up to 14 billion parameters) for real-time, streaming, and infinite-length audio-driven avatar generation without compromising visual fidelity. Our work successfully resolves the long-standing tension between high visual quality, model complexity, and practical execution speed through an algorithm-system co-design approach.

The core contributions of Live Avatar are as follows:

- **Causal, Streamable Adaptation Framework.** We employ Self-Forcing Distribution Matching Distillation to distill the knowledge from a non-causal model into a causal, few-step student architecture. This framework is designed to ensure the model’s efficiency for deployment on our subsequent distributed inference engine. Furthermore, during distillation, we inject random noise into the Key-Value cache of historical frames to enhance robustness in long-horizon video generation. This strategy not only mitigates quality degradation in long-term generation but also encourages the student model to draw upon

Method	stream	real time	inf-len	size
HalIo3[6]	✗	✗	✗	5B
StableAvatar[38]	✗	✗	✓	1.3B
Wan-s2v[15]	✗	✗	✗	14B
Ditto[24]	✓	✓	✓	0.2B
InfiniteTalk[47]	✗	✗	✓	14B
OminiAvatar[13]	✗	✗	✗	14B
Live avatar(ours)	✓	✓	✓	14B

Table 1. Comparison of state-of-the-art audio-driven avatar generation methods. Live Avatar simultaneously achieves streaming, real-time, and infinite-length generation with a high-fidelity, large-scale (14B) diffusion model.

the static identity features provided by the sink frame.

- **Timestep-forcing Pipeline Parallelism (TPP).** We introduce a novel distributed inference execution paradigm that physically decouples the sequential denoising steps across multiple devices. By assigning each device to a fixed timestep, we create a fully pipelined inference engine. This approach breaks the autoregressive denoising bottleneck inherent to diffusion models, achieving predictable low latency and guaranteeing 20 FPS real-time streaming performance on only  $5 \times$ H800 GPUs.
- **Rolling Sink Frame Mechanism (RSFM).** To tackle the challenge of long-term consistency, we propose RSFM. This mechanism dynamically recalibrates the generated sequence by periodically reintroducing and synchronizing the initial appearance frame during the generation process. RSFM effectively suppresses the accumulation of identity drift and color artifacts, ensuring high stability and visual coherence for streaming avatar video generation.

## 2. Related Works

**Streaming and Long Video Generation.** Streaming and long video generation require efficient management of both computation and memory resources. CausVid [50] applies distillation and KV cache to accelerate generation and enable streaming, but suffers from over-exposure artifacts caused by error accumulation over long sequences. Diffusion Forcing [3] introduces varied noise levels to sequential targets, supporting longer videos. Self Forcing [19] addresses exposure bias by conditioning on previously generated frames during training, resolving train-inference mismatches. Self-Forcing++ [7] extends DMD to support video generation beyond base model duration. LongLive [46] uses a KV-recache mechanism and short window attention for streaming and long-tuning. Rolling Forcing [26] proposes rolling window joint denoising and attention sink mechanisms for reduced error and improved coherence. StreamDiT [21] supports streaming and interactive gen-

eration using window attention and multistep distillation. While these approaches improve video quality and temporal consistency for long video generation, none achieve real-time, streaming long video generation with large-scale diffusion models.

**Audio-driven Avatar Video Generation.** Audio-driven avatar video generation requires subject consistency and effective motion control. Early works such as Wav2Lip [34] employ GANs for accurate lip-syncing, while SadTalker [52] predicts 3D motion coefficients from audio for flexible video control. With the success of diffusion models in video synthesis, several studies [37, 51] adapt diffusion frameworks and ReferenceNet architectures for audio-driven avatar generation, and DiT-based models are especially effective [2, 17, 22, 40]. Recently, more DiT-based approaches [8, 27, 32] have emerged, and some works [16, 24, 42, 53, 55] focus on head video generation due to the complexity of human motion. In addition, recent advances in autoregressive modeling for images, such as MAR [23], have inspired multimodal video generation methods [1, 4, 45] that combine autoregressive and diffusion strategies. Nevertheless, further progress is still required in maintaining identity consistency and achieving high video quality over long-form, audio-driven avatar video generation.

**Diffusion Distillation.** Diffusion model distillation has emerged as a pivotal technique for accelerating video generation. Classical distillation approaches include trajectory distillation[12], Consistency Models[28, 36, 54], and Distribution Matching Distillation (DMD)[30, 31, 49], all of which have demonstrated consistent benefits across diverse video generation models. In the context of streaming video generation, DMD has attracted broader attention. Notably, methods such as CausVID[50], Self-Forcing[7, 19], and LongLive[46] employ DMD for few-step distillation: they first generate long videos and subsequently extract temporal segments for DMD-based distillation. This strategy not only achieves significant sampling speedup but also substantially enhances the generation quality of minute-long videos. Recent works reveal that DMD can function analogously to reinforcement learning, where a pretrained diffusion model serves as a specialized reward signal during optimization[29], which may be the reason for the effectiveness of distillation on streaming video diffusion models.

The theoretical foundation of DMD is limited to single-step distillation. To address this limitation, TDM[31] establishes a trajectory-aware distribution matching framework that naturally extends to multi-step distillation, thereby achieving superior performance compared to DMD2[48].

### 3. Preliminaries

#### 3.1. Video Diffusion Models

Video diffusion models generate high-fidelity video sequences by progressively denoising from a Gaussian prior  $x_T \sim N(0, I)$ , following the reverse process of a forward diffusion. In this work, we adopt the flow matching [25], where noisy latents at time  $t$  are constructed as

$$x_t = (1 - s_t) \cdot x_0 + s_t \cdot x_T, s_t \in [0, 1] \quad (1)$$

is a scheduling function that controls the interpolation between clean and noise. The model is trained to predict the target velocity

$$v = x_T - x_0 \quad (2)$$

leading to the standard mean squared error objective:

$$\mathcal{L} = \mathbb{E}_{x_0, x_T, t} [\|v_\theta(x_t, t, c) - (x_T - x_0)\|_2^2] \quad (3)$$

where  $c$  denotes conditional inputs such as text embeddings.

To reduce computational cost, most modern video diffusion models operate in a compressed latent space. We use a causal 3D VAE to encode input videos into temporal-latent representations, ensuring that future frames do not leak during training. Text conditioning is achieved through a pre-trained language model that produces contextual embeddings fed into the diffusion backbone.

#### 3.2. Distribution Matching Distillation

Distribution Matching Distillation (DMD)[49] aims to distill a pre-trained teacher diffusion model into a student model that operates with fewer sampling steps. Let  $p_{\theta, t}(\mathbf{x}_t)$  denote the distribution induced by the few-step student model  $\mathbf{x} = G_\theta(\mathbf{z})$ , and let  $p_{\text{data}, t}(\mathbf{x}_t)$  represent the corresponding ground-truth distribution produced by the teacher diffusion model at time step  $t$ . The primary objective of DMD is to minimize the distribution, i.e., reverse Kullback–Leibler (KL) divergence, between these two distributions at each time step  $t$ :  $\mathbb{E}_t [D_{\text{KL}}(p_{\theta, t} \parallel p_{\text{data}, t})]$ . The gradient of DMD loss is given by:

$$\nabla_\theta \mathcal{L}_{\text{DMD}} = -\mathbb{E}_{t, \mathbf{z}} \left[ (s_{\text{real}}(\mathbf{x}_t, t) - s_{\text{fake}, \phi}(\mathbf{x}_t, t))^\top \frac{\partial G_\theta(\mathbf{z})}{\partial \theta} \right] \quad (4)$$

where  $\mathbf{x}_t = \Psi(\hat{\mathbf{x}}, t)$  is the noise scheduler,  $\hat{\mathbf{x}} = G_\theta(\mathbf{z})$  is the data prediction of the distilled model,  $s_{\text{real}}$  and  $s_{\text{fake}, \phi}$  denote the score functions corresponding to the pre-trained teacher diffusion model and the student generator, respectively.

$s_{\text{real}}$ ,  $s_{\text{fake}, \phi}$ , and  $G_\theta(\mathbf{z})$  are all initialized from the pre-trained teacher model induced by  $v_\theta$ . The training proceeds by alternately updating  $s_{\text{fake}, \phi}$  and  $G_\theta(\mathbf{z})$ , in which  $s_{\text{fake}, \phi}$  is trained on samples generated by the current student generator  $G_\theta(\mathbf{z})$ , and  $G_\theta(\mathbf{z})$  is trained using the DMD loss defined above. For multi-step distillation, DMD first performs

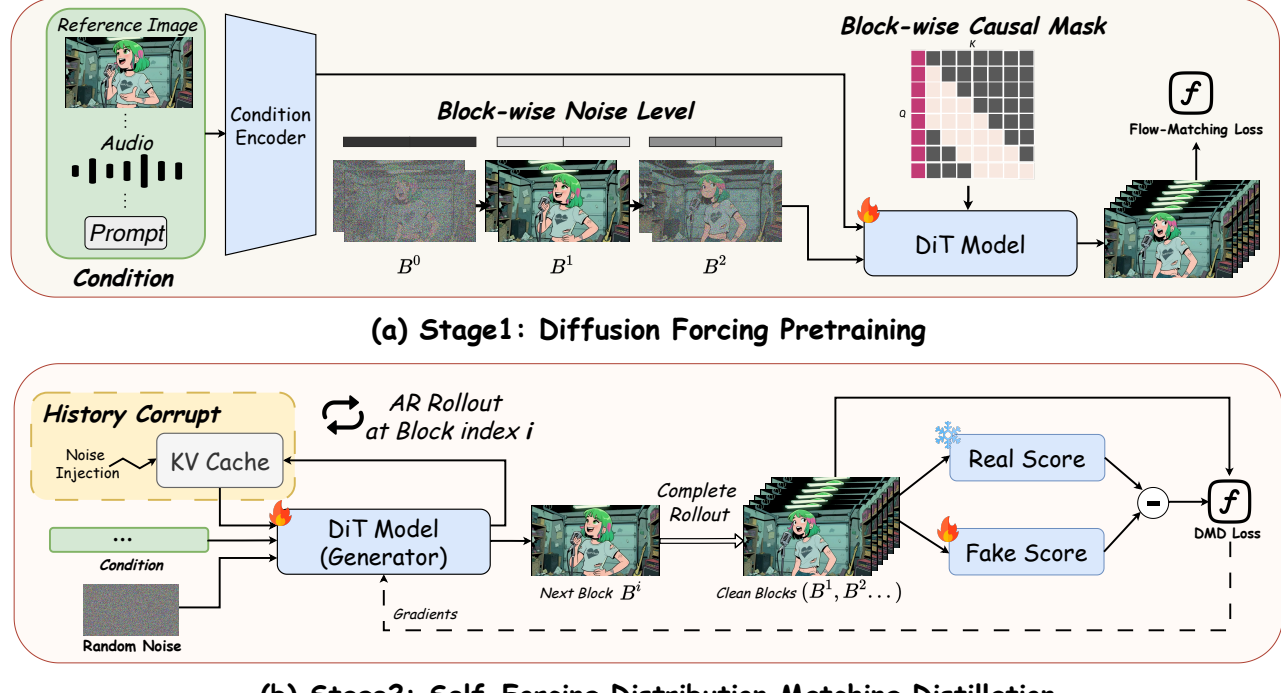


Figure 2. The Live Avatar Training Framework. (a) Stage 1 Diffusion Forcing Pretraining, showing the block-wise noise setup and the applied attention masks. (b) Stage 2 Self-Forcing Training, where the noise level consistency between the KV cache and the noisy latents is enforced for distillation.

a multi-step sampling trajectory using the student generator:  $\mathbf{z} \xrightarrow{G_\theta} \hat{\mathbf{x}}_{t_1} \xrightarrow{\Psi} \mathbf{x}_{t_1} \xrightarrow{G_\theta} \hat{\mathbf{x}}_{t_2} \xrightarrow{\Psi} \mathbf{x}_{t_2} \rightarrow \dots \rightarrow \mathbf{x}_{t_N}$ . Then, at each training iteration, a random intermediate state  $\mathbf{x}_{t_i}$  from this trajectory is selected and used in place of pure noise  $\mathbf{z}$  as the starting point for the DMD training procedure.[48]

## 4. The Live Avatar Framework

In this section, we present the technical details of Live Avatar. We first detail the model architecture in Sec.4.1, following overall training framework in Sec.4.2 and Fig. 2. The inference framework and Timestep-forcing Pipeline are demonstrated in Sec.4.3. We also investigate long video generation in Section 4.4 and propose the rolling sink frame to address identity inconsistency and color artifacts in long-term generation.

### 4.1. Model Architecture

In order to enable streaming video generation, the Live Avatar adopt autoregressive generation by factorizing the joint distribution

$$B_{t-1}^i = v_\theta(B_t^i, \underbrace{B_t^{(i-w):(i-1)}}_{\text{kv cache}}, I, a^i, t^i) \quad (5)$$

combining diffusion-based frame synthesis with causal dependencies across chunks.  $B$  in Eq.5 are blocks of consecutive noisy frame latents. In our work, we set the number of frame latents to 3; Here, the  $I$  denotes the rolling sink frame, which provides the appearance;  $a^i$  and  $t^i$  are the audio embedding and prompt embedding for the  $i$ -th block respectively. The underscore  $t$  denotes the denoising step, and the superscript  $i$  denotes the frame index. Note that in the model, the kv cache  $B_t^{(i-w):(i-1)}$  and the noisy block  $B_t^i$  share the same noise level, this is a crucial design that improves generation quality and maximize the inference speed, which will be illustrated in Sec.4.3.

### 4.2. Model Training

Our overall training framework is illustrated in Figure 2, which consists of two main stages: 1) Stage 1, **Diffusion Forcing Pretraining** with a block-wise independent noise scheduling and causal local attention mask, and 2) stage 2, **Self-Forcing Distribution Matching Distillation** with KV cache perturbation.

In the first stage, we perform diffusion-forcing pretraining to ensure stable training in the next distillation stage. We apply causal masks during training following CausVid[50] and X-Streamer[45]. The masking strategy treats all frames within a block as fully visible (i.e., intra-block full attention).

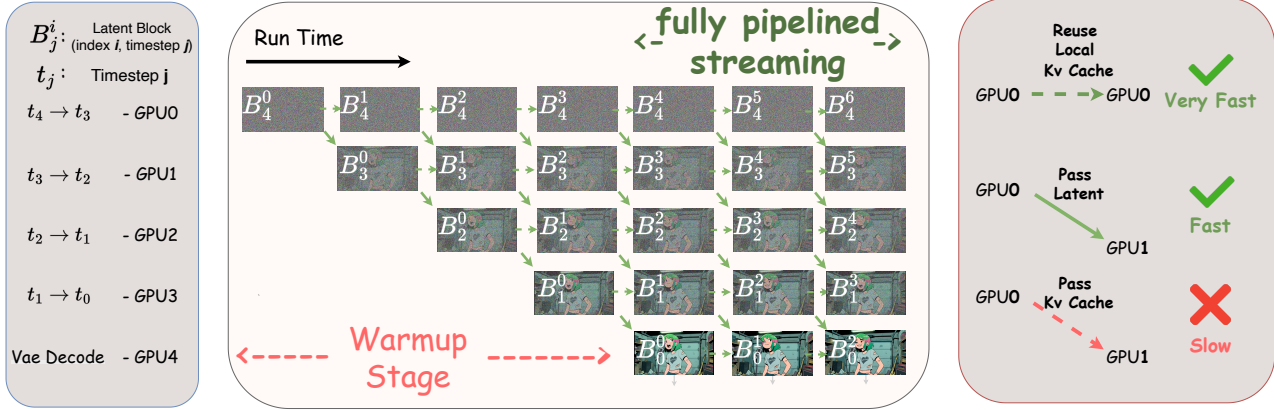


Figure 3. A visual illustration of Timestep-forcing Pipeline Parallelism (TPP). After warm-up fills the pipeline, all GPUs denoise **simultaneously** in the fully pipelined stage, turning the sequential diffusion chain into an asynchronous spatial pipeline. For example, GPU2 always performs the  $t_2 \rightarrow t_1$  step: it reuses its local KV cache (**very fast**) and sends only the latent to GPU3 (**fast**).

tion), while enforcing causality between blocks, each block can only attend to features from earlier blocks(i.e., inter-block causal attention).

In the second stage, we distill the knowledge of a bidirectional teacher model into a causal, few-step generator suitable for efficient streaming avatar video synthesis. Our approach builds upon the Self-forcing paradigm [19], involving three key models during training: (1) a fixed bidirectional diffusion teacher (Real Score Model), which represents the target distribution; (2) a dynamically updated bidirectional model (Fake Score Model) that tracks the distribution of the student generator’s outputs; and (3) a causal, autoregressive generator that is initialized from the first stage model and optimized for few steps denoising.

A primary technical challenge arises from the need to generate long-sequence latent inputs for the bidirectional score models in a fashion that is compatible with causal, block-wise streaming generation. To address this, the causal generator produces the video sequence autoregressively, denoising one block at a time while conditioning on previous blocks. After each block is synthesized, the clean latent is stored, and the sequence of these latents forms the input trajectory for both Real and Fake Score Models. Specifically, we follow self-forcing[19] and apply holistic distribution-matching loss in an online manner. To ensure tractable memory usage during training, we adopt computation graph truncation as introduced in the self-forcing.

Maintaining long-sequence coherence and stability is further facilitated by introducing a Key-Value (KV) caching strategy within the causal architecture. At each denoising step, KV activations are cached and propagated across blocks, preserving temporal context. Specifically, during the denoising of each block, the model attends to the KV cache from previous blocks at the same timestep, following the practice introduced in [27]. To further boost robustness,

we inject random noise into the historical KV cache, which we refer to as **History Corrupt**<sup>1</sup>. This noise injection encourages the model to distinguish between dynamic motion from recent history and the static identity cues contributed by the sink frame, ultimately supporting stable, high-quality video streaming over arbitrary durations, thereby improving temporal coherence and reducing artifact accumulation across the video sequence.

### 4.3. Timestep-forcing Pipeline Parallelism

Deploying large video generation models in real-time settings remains challenging due to the inherent sequential structure of diffusion-based sampling. Our distilled 14B model, for example, reaches only 5 FPS on a single GPU and 6 FPS under conventional 4-GPU sequential parallelization. In contrast, existing real-time streaming methods, such as CausVid [50] and LongLive [46], achieve higher frame rates by substantially reducing model capacity—often relying on lightweight 1.3B models and aggressive quantization—at the cost of generation fidelity. This establishes a long-standing tradeoff between model quality and real-time performance that has yet to be resolved.

To overcome the sequential bottleneck of diffusion sampling, we introduce **Timestep-forcing Pipeline Parallelism (TPP)** (illustrated in Figure 3), which assigns each GPU a fixed timestep  $t_i$  and partitions the  $T$  denoising steps across  $T$  devices. Each GPU repeatedly performs its designated transformation  $t_i \rightarrow t_{i-1}$ , converting the Sequential diffusion chain into an asynchronous spatial pipeline. Through this reparameterization, throughput is determined by the single denoise forward of the model rather than the sum of all diffusion steps, effectively removing the inference-time sampling bottleneck. TPP enables real-time

<sup>1</sup>Details of History Corrupt are provided in the supplementary materials.

streaming generation at over 20 FPS while preserving the capacity and quality benefits of multi-step diffusion.

TPP operates in two stages. During warm-up, the first block is propagated through all timesteps to fill the pipeline, which completes quickly given the small number of sampling steps. Once filled, the system enters the fully pipelined streaming phase: each GPU repeatedly performs its assigned denoising step, passes the latent to the next device, and immediately processes the next block, achieving maximal parallel throughput. Each GPU maintains its own rolling KV cache. This design both enables TPP and aligns with the base-model’s pretraining-time setting, which helps stabilize generation quality [27]. At each denoising step,  $GPU_i$  reuses its local KV cache, attending only to the KV cache within its predefined local window. This operation is entirely local—requiring no inter-GPU communication—and thus remains extremely fast and efficient. After finishing its step,  $GPU_i$  passes only the latent to  $GPU_{i+1}$ , keeping the communication cost negligible. To prevent pipeline bottlenecks, the VAE decoding stage is offloaded to an additional dedicated GPU, which consumes the clean latent and outputs synchronized video chunks.

#### 4.4. Rolling Sink Frame for long video generation

Existing talking-avatar systems exhibit pronounced degradation over long, streaming runs—manifesting as identity drift, color shifts, and temporal instability [38]. In practice we run inference in a rolling-KV-cache [19], which extends the temporal horizon but does not by itself prevent collapse. We attribute these long-horizon failures to two internal phenomena. First, **inference-mode drift**: the conditioning pattern at inference (e.g., the RoPE-relative positioning between the sink frame and current target blocks) gradually diverges from the training-time setup, weakening identity cues. Second, **distribution drift**: the distribution of generated frames progressively deviates from normal, realistic video distributions, likely driven by persistent factors that continuously push the rolling generation toward unrealistic outputs. To address these challenges, we propose the **Rolling Sink Frame Mechanism (RSFM)**, a unified approach that maintains a single, dynamically aligned sink frame throughout generation to ensure long-term consistency and fidelity.

To counteract distribution drift, we propose **Adaptive Attention Sink (AAS)**<sup>2</sup>: immediately after the first block is generated, we replace the original sink frame with the model’s own first generated frame (VAE-encoded) and use that frame as the persistent sink for subsequent conditioning. By keeping the sink frame within the model’s learned generation distribution, AAS mitigates the persistent factors that would otherwise push the video toward unrealistic

<sup>2</sup>Details of AAS and Rolling RoPE are provided in the supplementary materials.

color, exposure, or style deviations, while preserving identity cues.

To mitigate inference-mode drift, we introduce **Rolling RoPE**<sup>2</sup>, a dynamic position-alignment mechanism for the sink frame. The sink frame is permanently cached in KV cache and its temporal offset is adjusted via a controllable RoPE shift so that its relative position to the current noisy states remains consistent with training. This dynamic RoPE alignment lets the model continuously reference identity features from sink frame without rigidly constraining local motion, thereby stabilizing long-range identity and structural fidelity.

## 5. Experiments

### 5.1. Experimental Settings

**Implementation Details** The overall model architecture is borrowed from WanS2V [15], but the framepack is removed for conciseness. In stage 1, we initialize from its weights. In stage 2, the teacher score and fake score branches are initialized from Wan-S2V, while the student is initialized from Stage 1. All training and inference are performed at a fixed resolution of 720×400 and 84 frames. Experiments are conducted on 128 NVIDIA H800 GPUs, with 25 K and 2.5 K steps for stage 1 and stage 2, respectively, totaling about 500 GPU days. The per-GPU batch size is 1. To handle the high memory demand of Self-Forcing training, we adopt FSDP with gradient accumulation to reduce memory consumption. The learning rate is 1e-5 for the student and 2e-6 for the fake score. We group every 3 frames into a block, set the KV cache length to 4 blocks, and use a single rolling sink frame. We train models with a LoRA, whose rank and alpha are set to 128 and 64, respectively.

**Datasets** We train our model on the AVSpeech[10] dataset, a large-scale audio-visual corpus comprising numerous video clips of human subjects with synchronized audio. To ensure data quality and maintain consistency with prior work, we follow the data preprocessing protocol established by OmniAvatar[13]. Additionally, we filter the raw data, retaining only video segments longer than 10 seconds for training. This process yields a final training set of 400,000 high-quality samples. To evaluate our model’s out-of-domain (OOD) generalization, we created a synthetic benchmark named GenBench. This test set was generated using Gemini-2.5 Pro, Qwen-Image[43], and CosyVoice[9]. It is composed of two subsets: GenBench-ShortVideo, comprising 100 test samples with an approximate duration of 10 seconds, and GenBench-LongVideo, which contains 15 test videos, each exceeding 5 minutes in duration. The benchmark is designed to be challenging, featuring a wide diversity of character styles (photorealistic humans, animated characters, and anthropomorphic non-humans) and visual compositions, including frontal and profile views, as well

Table 2. Quantitative comparisons of our methods with state-of-the-art methods.

Dataset	Model	Metrics					
		ASE $\uparrow$	IQA $\uparrow$	Sync-C $\uparrow$	Sync-D $\downarrow$	Dino-S $\uparrow$	FPS $\uparrow$
GenBench-ShortVideo	Ditto[24]	3.31	4.24	4.09	10.76	0.99	21.80
	Echomimic-V2[33]	2.82	3.61	5.57	9.13	0.79	0.53
	Hallo3[6]	3.12	3.97	4.74	10.19	0.94	0.26
	StableAvatar[38]	3.52	4.47	3.42	11.33	0.93	0.64
	OmniAvatar[13]	3.53	4.49	6.77	8.22	0.95	0.16
	WanS2V[14]	3.36	4.29	5.89	9.08	0.95	0.25
	Ours	3.44	4.35	5.69	9.13	0.95	20.88
GenBench-LongVideo	Ditto[24]	2.90	4.48	3.98	10.57	0.98	21.80
	Hallo3[6]	2.65	4.04	6.18	9.29	0.83	0.26
	StableAvatar[38]	3.00	4.66	1.97	13.57	0.94	0.64
	OmniAvatar[13]	2.36	2.86	8.00	7.59	0.66	0.16
	WanS2V[14]	2.63	3.99	6.04	9.12	0.80	0.25
	Ours	<b>3.38</b>	<b>4.73</b>	6.28	8.81	0.94	20.88

as half-body and full-body shots. This variety allows for a robust assessment of the model’s performance on unseen data.

**Evaluation Metrics** To evaluate our model, we assess frame-level image quality using FID[18] and overall video coherence with FVD[39]. For audio-visual synchronization, we measure the correspondence between lip movements and the input audio using Sync-C and Sync-D metrics[5]. Additionally, we employ the Q-align[44] model to evaluate the final video’s perceptual quality (IQA) and aesthetic appeal (ASE). For our custom Out-of-Distribution (OOD) test set, we only compute Sync-C, Sync-D, IQA, and ASE, as ground truth videos are unavailable.

## 5.2. Comparison with Existing Methods

We compare Live Avatar against current state-of-the-art open-sourced audio-driven avatar generation approaches, including Ditto[24], Echomimic-V2[33], StableAvatar[38], OmniAvatar[13], and WanS2V[14]. Quantitative results on relevant objective metrics are presented in Table 2. In terms of visual quality, our method achieves competitive performance in ASE and IQA, comparable with OmniAvatar and Stable-Avatar and performs better than Ditto, Echomimic-V2 and WanS2V. Notably, although our approach is built upon WanS2V and employs step distillation, it demonstrates superior base visual quality compared to WanS2V. This observation aligns with findings in prior work utilizing DMD, where the DMD loss has been interpreted as a specialized reinforcement learning objective that effectively optimizes both aesthetic appeal and foundational visual fidelity[29, 31]. Regarding audio-visual synchronization, our method also performs favorably, better than Ditto, Echomimic-V2 and StableAvatar and trailing only slightly behind WanS2V and OmniAvatar. This result is understand-

able given that step distillation inherently incurs some loss of dynamic temporal information[11]. The advantage of inference speed over WanS2V and OmniAvatar is the most favorable.

More significantly, our method exhibits a pronounced advantage in long-duration video generation. As shown in Table 2, which presents results for 7-minute-long videos, our approach substantially outperforms all baselines across almost every evaluation metric, especially on ASE and IQA. Qualitative visualizations in Figure 4 further corroborate this finding: existing methods, especially OmniAvatar and WanS2V, suffer from noticeable degradation in visual quality over extended durations, whereas our method consistently maintains high base-level visual fidelity throughout the entire sequence.

Table 3. Ablation Study on Inference Efficiency. TTFF measures the **end-to-end** time-to-first-frame, which includes the VAE decoding time. Note that  $SP_{4GPU}$  indicates a sequence parallelism of 4 GPUs.

Methods	#GPUs	NFE	FPS $\uparrow$	TTFF $\downarrow$
w/o TPP	2	5	4.26	3.88
w/o TPP, w/ $SP_{4GPU}$	5	5	5.01	3.24
w/o VAE Parallel	4	4	10.16	4.73
w/o DMD	2	80	0.29	45.50
Ours	5	4	<b>20.88</b>	<b>2.89</b>

## 5.3. Ablation Study

**Study of Inference efficiency** We analyze the impact of the Live Avatar model architecture and inference strategies on generation latency, considering the following variants: (1) Timestep-forcing Pipeline Parallelism (TPP), (2) disabling multi-GPU parallelism (denoted as w/  $SP_{4GPU}$ ), (3) dis-

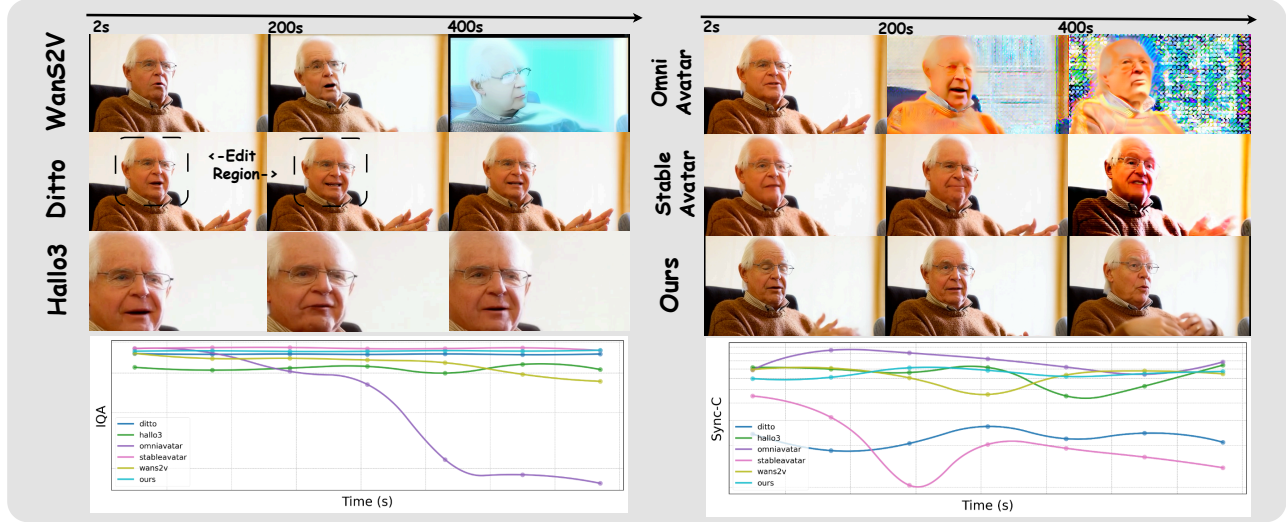


Figure 4. Qualitative comparisons with state-of-the-art methods.

Table 4. Ablation Study on Long Video Generation.

Methods	Metrics			
	ASE $\uparrow$	IQA $\uparrow$	Sync-C $\uparrow$	Dino-S $\uparrow$
w/o AAS	3.13	4.44	6.25	0.91
w/o Rolling RoPE	<b>3.38</b>	4.71	<b>6.29</b>	0.86
w/o History Corrupt	2.90	3.88	6.14	0.81
Ours	<b>3.38</b>	<b>4.73</b>	6.28	<b>0.93</b>

abling VAE parallelization, and (4) using Diffusion-forcing alone without DMD.

We evaluate inference efficiency along two dimensions: (i) frames-per-second (FPS), defined as the average number of video frames generated per second, and (ii) the time-to-first-frame (TTFF), i.e., the end-to-end latency to generate the first output frame. The corresponding results are summarized in Table 3.

As shown in the table, DMD yields the most significant improvement in both FPS and TTFF, primarily due to its substantial reduction in the number of function evaluations (NFE). If TPP is discarded, there is a remarkable throughput reduction to only 4 FPS. Moreover, employing sequence parallelism across GPUs provides only marginal gains in efficiency, which may stem from the fact that the inference sequence length per latent frame block is short and the computational cost is no longer the dominant factor in overall latency. Consequently, the VAE decoding latency constitutes a non-negligible bottleneck for real-time generation, making parallelizing the VAE decoding a critical design choice.

**Study on effectiveness of Rolling Sink Frame on long video generation** Rolling Sink Frame is a key inference technique enabling high-quality long-duration video generation. As shown in Table 4, removing both the Adap-

tive Attention Sink and the History Corrupt strategy leads to a sharp decline in ASE and IQA scores, indicating that these components are crucial for maintaining perceptual and temporal consistency over minute-scale generations. Furthermore, discarding Rolling RoPE results in drop in the DINOv2 similarity metric. This suggests that Rolling RoPE plays an essential role in preserving semantic consistency between the current frame and the sink frame, thereby safeguarding global semantic attributes, especially identity, throughout extended sequences.

#### 5.4. User Study

Prior work such as THEval [35] has shown that popular metrics for talking-avatar evaluation (e.g., Sync-C) often diverge from human perception, as models can exploit them by exaggerating lip motion. To bridge this gap, we conduct a double-blind user study with 20 participants, who rate generated videos from all methods on Naturalness, Synchronization, and Consistency. Here, Synchronization refers to the holistic audiovisual coherence [41]—including facial expressions, gestures, and posture transitions—rather than the frame-level lip alignment measured by Sync-C. The final scores are averaged across participants and normalized to a 0–100 scale for comparison. As summarized in Table 5, although OmniAvatar achieves the best objective metrics, it is rated significantly lower by human evaluators, confirming that over-optimized lip movements harm perceptual naturalness. In contrast, our method attains the most balanced scores across all criteria, suggesting better alignment with human perception of natural and coherent motion. EchoMimic V2, which relies on fixed hand-landmark templates, shows degraded scores as it struggles to generalize to diverse body poses, often resulting in distorted ges-

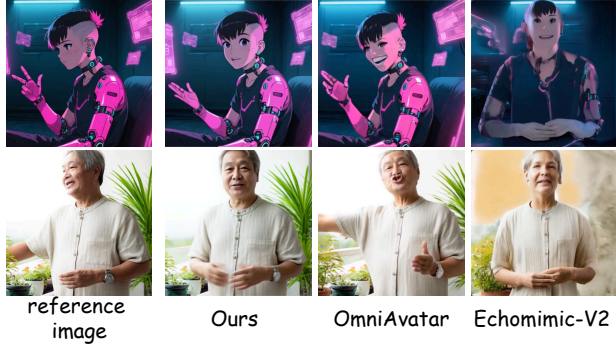


Figure 5. Qualitative Comparison of Our Model, OmniAvatar, and Echomimic-v2. Results are sampled from GenBench-ShortVideo.

tures. In contrast, our method is consistently preferred by human evaluators, indicating stronger alignment with human perception of natural and coherent motion. The results of the visualization are presented in 5 .

Table 5. User study results on perceptual evaluation (higher is better). Each score denotes the mean normalized user rating.

Model	Naturalness $\uparrow$	Synchronization $\uparrow$	Consistency $\uparrow$
Ditto [24]	78.2	40.5	90.2
EchoMimic-V2 [33]	60.3	71.1	38.7
Hallo3 [6]	78.5	69.2	89.3
StableAvatar [38]	68.7	70.8	88.9
OmniAvatar [13]	71.1	78.5	90.8
WanS2V [14]	84.3	<b>85.2</b>	<b>92.0</b>
Ours	<b>86.3</b>	80.6	91.1

## 6. Conclusion

In this work, we present **Live Avatar**, a novel algorithm-system co-designed framework that effectively bridges the gap between high-fidelity audio-driven avatar generation and real-world deployment requirements. By simultaneously addressing the two core challenges, i.e. real-time inference latency and long-horizon visual consistency, Live Avatar enables, for the first time, efficient streaming inference with large-scale diffusion models of up to 14 billion parameters without compromising visual realism or expressiveness. Specifically, through key techniques, our system achieves stable real-time streaming at 20 FPS using only 5 H800 GPUs. Meanwhile, the Rolling Sink Frame Mechanism effectively suppresses identity drift and color artifacts that typically accumulate during prolonged generation, significantly enhancing visual coherence and stability. To conclude, Live Avatar is capable of real-time, infinite-length, high-quality audio-driven avatar video generation, laying a solid foundation for the practical deployment of next-generation interactive digital humans.

**Limitation** The proposed TPP inference strategy en-

hances FPS but does not reduce TTFF, thereby limiting interactive responsiveness. In addition, the strong dependence on RSFM may compromise long-term temporal consistency in complex scenarios. Future work will focus on reducing latency and improving temporal coherence.

# Live Avatar: Streaming Real-time Audio-Driven Avatar Generation with Infinite Length

## Supplementary Material

### 7. Overview of Supplementary Material

This supplementary document provides comprehensive details, additional experiments, and implementation specifics to support the findings in the main paper. The content is organized as follows:

- **Section 9: Additional Experimental Results.** We investigate the impact of KV cache noise levels (Table 6), evaluate our model’s long-horizon autoregressive extrapolation up to 10000s (Table 7, Figure 9), and further provide additional comparision against State-of-The-Art on AV-Speech test set (Table 8).
- **Section 10: Additional Experimental Setting.** We detail the hardware configurations, inference configurations, and specific definitions for runtime metrics used in our benchmarking.
- **Section 11: Algorithm Details.** We provide complete pseudocode (Algorithm 1, 2, 3 and 4) for our methods, including the *History Corrupt* and *Block-wise Gradient Accumulation* training strategies, and detailed inference procedures for single-GPU setups (incorporating AAS and Rolling RoPE) and multi-GPU TPP. We further include visualizations (Figures 6, 7, and 8) to illustrate the mechanisms of different inference settings.
- **Section 12: Additional Visual Results.** We showcase further qualitative examples to demonstrate the temporal consistency and visual fidelity of our method.
- **Section 13: Ethical Consideration.** We discuss the potential societal impacts, privacy concerns, and responsible usage guidelines for our audio-driven avatar generation framework.

### 8. LLM USAGE STATEMENT.

We use LLMs (e.g., Gemini-2.5 and GPT-5) to polish our paragraphs.

### 9. Additional Experimental Results.

#### 9.1. Does the Noise Level of KV Caches Matter?

Prior streaming systems such as CausVid [50], LongLive[46], and Self-Forcing [19] typically use clean KV caches, an intuitive choice given their higher information content. However, recent diffusion-based avatar models (e.g., TalkingMachine, StableAvatar) implicitly rely on same-timestep (same-noise) KV caches, without discussing why this design works or whether it is preferable. This motivates our study of a simple question: does the noise level of the KV caches actually matter for streaming diffusion models?

To answer this, we compare two settings: (1) **Timestep-forcing**, where each GPU handles one timestep and every noisy latent attends only to the KV cache of the same noise level. (2) **Clean-kv-cache**, where all latents attend to a unified clean cache that must be generated via an extra forward pass (Algorithm 2 in [50]), introducing an additional 1 NFE. Since the clean cache for frame  $t+1$  depends on the fully denoised output of frame  $t$ , each frame must wait for the previous one to finish before denoising can begin. Consequently, autoregressive generation cannot exploit pipeline parallelism and is limited to conventional sequential parallelism across GPUs, leading to substantial efficiency degradation. All experiments use four H800s and report both efficiency (FPS, TTFF) and quality (ASE, IQA, Sync-C, Sync-D, Dino-S).

Results in Table 6 show that timestep-forcing (which also enable TPP) consistently outperform clean-kv-cache not only in efficiency—as discussed above—but also in perceptual quality. We attribute the quality improvement to model’s pre-training: diffusion video models primarily learn cross-frame attention under same-timestep conditions, making noise-aligned KV features a closer match to the learned denoising distribution. In addition, the TPP setting is far more scalable, as it avoids all inter-GPU KV communication, whereas the clean-KV alternative incurs substantial synchronization cost and higher latency.

#### 9.2. Extending Autoregressive Generation to 10,000 Seconds.

To rigorously evaluate the long-horizon autoregressive capability of our model, we construct a stress test far exceeding the temporal range seen during training. Although the model is trained exclusively on 5-second clips—and its RoPE positions

Table 6. Quantitative comparisons of timestep-forcing with traditional clean-kv-cache.

Dataset	Model	Metrics							
		#GPUs	NFE $\downarrow$	ASE $\uparrow$	IQA $\uparrow$	Sync-C $\uparrow$	Sync-D $\downarrow$	Dino-S $\uparrow$	FPS $\uparrow$
GenBench-ShortVideo	clean-kv-cache	4	5	3.26	4.01	<b>5.69</b>	9.53	0.93	5.01
	timestep-forcing	4	<b>4</b>	<b>3.44</b>	<b>4.35</b>	5.62	<b>9.13</b>	<b>0.95</b>	<b>20.88</b>
GenBench-LongVideo	clean-kv-cache	4	5	3.05	4.44	6.11	9.10	0.90	5.01
	timestep-forcing	4	<b>4</b>	<b>3.38</b>	<b>4.73</b>	<b>6.28</b>	<b>8.81</b>	<b>0.94</b>	<b>20.88</b>

during training are randomly shifted only within a short-range window of a few minutes—we extend inference to an extreme 10,000-second horizon. Each audio input in GenBench-LongVideo ( $\approx$  10 minutes per sample) is repeated to match this duration, ensuring valid conditioning over the full sequence while avoiding degenerate periodicity. The model then performs fully autoregressive, block-wise generation like Self-Forcing [19], relying entirely on accumulated KV caches and our Rolling-RoPE strategy throughout the 10,000-second rollout.

This setup intentionally exposes the model to RoPE indices over two orders of magnitude larger than those encountered in training (10k seconds corresponds to RoPE positions around 40k), a regime where existing methods typically suffer severe attention degradation, ID drift, or visual collapse. Self-Forcing++ [7] demonstrates video generation of roughly 4 minutes, representing the longest horizon reported in prior work. In contrast, our model shows no observable quality decay or identity instability over the entire 10,000-second sequence. As shown in Table 7, perceptual quality (ASE, IQA), audio–visual synchronization (sync-C), and semantic consistency (DINO-s) remain nearly unchanged across segments sampled at 0–10 s, 100–110 s, 1000–1010 s, and 10000–10010 s. Figure 9 provides a representative case, demonstrating consistent identity and visual fidelity even at the 10k-second horizon.

Together, these results indicate that our long-video generation strategies—AAS, history corruption, and Rolling-RoPE—allow the model to stably extrapolate far beyond its training regime, achieving an unprecedented 10,000-second autoregressive rollout without quality degradation.

Table 7. Ablation Study on Long Video Generation.

Methods	Metrics			
	ASE $\uparrow$	IQA $\uparrow$	Sync-C $\uparrow$	Dino-S $\uparrow$
0-10s	3.37	<b>4.72</b>	6.20	<b>0.94</b>
100-110s	<b>3.38</b>	4.71	<b>6.44</b>	0.93
1000-1010s	3.37	4.69	5.98	0.93
10000-10010s	<b>3.38</b>	4.71	6.26	0.93

### 9.3. Additional Comparison with Existing Methods.

Although we have already provided comprehensive comparisons on GenBench in the main paper, we further evaluate the robustness of our method within its training domain, AVSpeech. Specifically, we hold out 5% of the original training videos and randomly sample 50 clips (5–10 seconds each) from this subset as an unseen test set. We report the same metrics used in the main evaluation; additionally, since ground-truth videos are available for this test set, we include FID and FVD to assess distribution alignment more thoroughly. The results are presented in Table 8.

The results in Table 8 show that our method achieves competitive or superior performance across most metrics on the in-domain AVSpeech evaluation. Notably, OmniAvatar is also trained on AVSpeech and therefore serves as a strong in-domain baseline, yet our method remains competitive under this setting. Together with the results reported on multiple public benchmarks in the main paper, this additional experiment verifies that our approach performs reliably within its training domain and alleviates potential concerns about relying solely on benchmark-specific evaluations.

## 10. Additional Evaluation Details.

**Inference Configuration.** All methods are evaluated on a single H800 node under identical hardware conditions. To ensure fair comparison, we utilize multi-GPU parallel inference for all methods where the official open-source code provides ap-

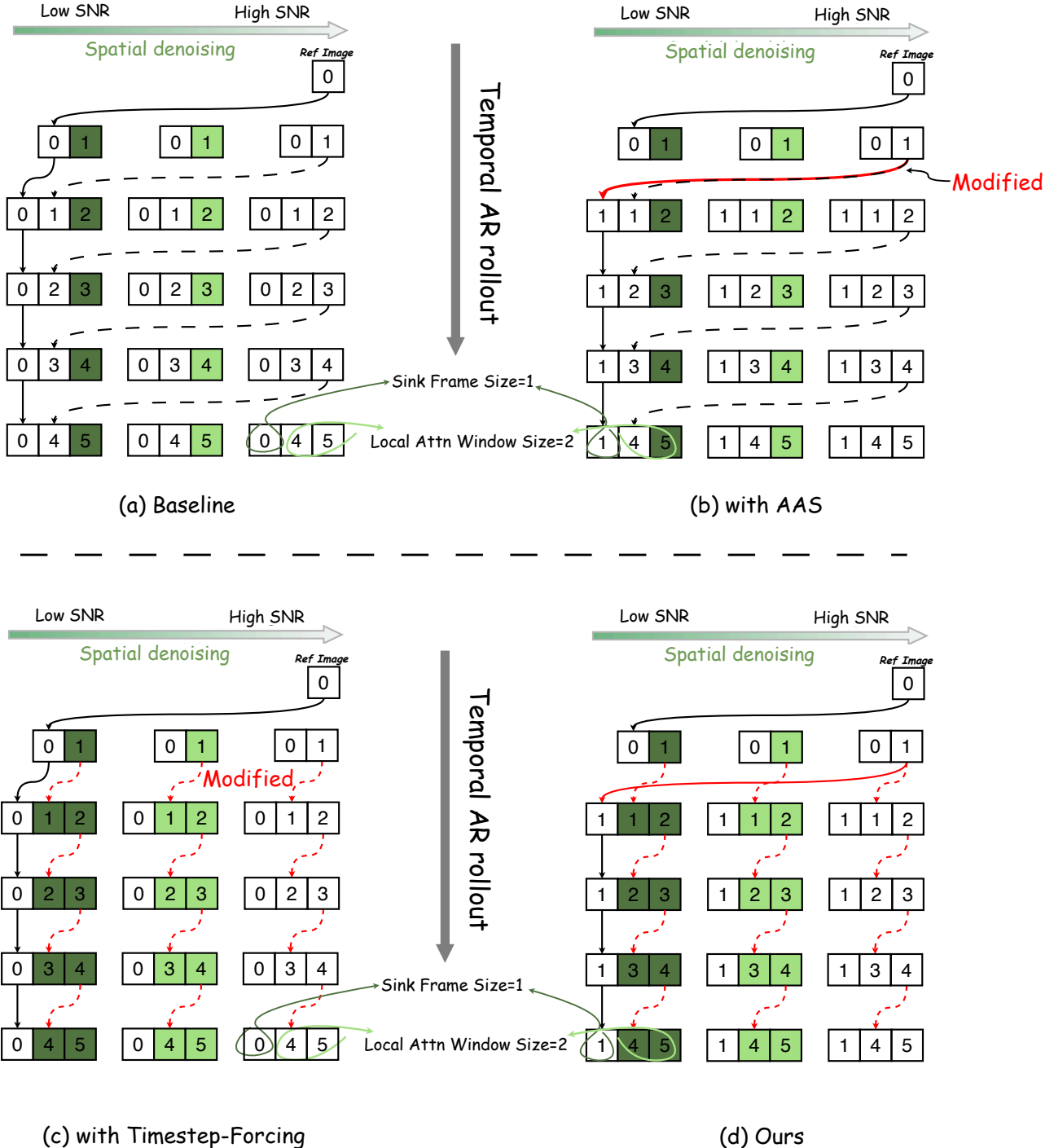


Figure 6. Illustration of different inference settings. Horizontally, each row follows the spatial denoising order from low to high SNR; vertically, each column shows the autoregressive rollout over frames. Each small **rectangle** denotes the latent of a block, and the **number** inside represents its block index. **Solid arrows** indicate direct sink frame passing, whereas **dashed arrows** indicate KV-cache passing. **Red** marks indicate the components modified relative to the baseline. (a) Baseline with a fixed sink frame and standard rolling-kv-cache. (b) AAS with the sink replaced by the first generated latent. (c) **Timestep-forcing** with each noisy latent attending only to KV caches of the same timestep. (d) **Ours** with both AAS and timestep-forcing.

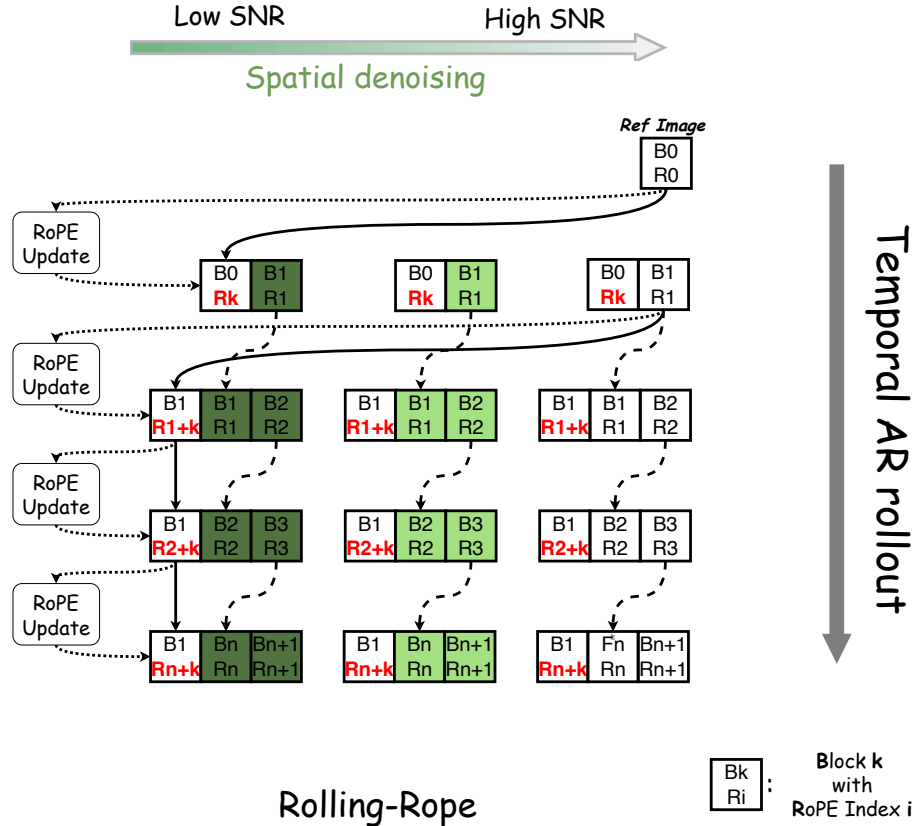


Figure 7. Visualization of the proposed Rolling-RoPE mechanism. Horizontally, each row follows the spatial denoising order from low to high SNR; vertically, each column shows the autoregressive rollout over frames. Each small **rectangle** denotes the latent of a block, and the **number** inside represents its block index and its RoPE index, respectively. **Red** marks indicate the components modified relative to the baseline. **Solid arrows** denote sink-frame passing, **sparse dashed arrows** denote standard KV-cache passing, and **dense dashed arrows** indicate RoPE updates, where each block is reassigned a updated positional embeddings. Rolling-RoPE dynamically **increases the RoPE index** of the sink frame throughout AR rollout, keeping the sink frame’s RoPE index slightly larger than that of the current noisy block, ensuring a stable and appropriate relative positional distance throughout AR rollout.

Table 8. Quantitative comparisons of our methods with other methods.

Dataset	Model	Metrics							
		FID $\downarrow$	FVD $\downarrow$	ASE $\uparrow$	IQA $\uparrow$	Sync-C $\uparrow$	Sync-D $\downarrow$	Dino-S $\uparrow$	FPS $\uparrow$
AV-Speech	Ditto[24]	<b>46.27</b>	660.01	2.21	3.75	4.84	9.05	0.99	21.80
	Echomimic-V2[33]	176.74	2059.81	1.88	3.29	4.07	9.38	0.78	0.53
	Hallo3[6]	138.40	1412.93	1.87	3.35	4.50	9.99	0.93	0.26
	StableAvatar[38]	98.32	730.12	2.14	3.55	5.72	9.01	0.93	0.64
	OmniAvatar[13]	50.42	570.32	2.16	3.68	<b>6.04</b>	<b>8.37</b>	<b>0.95</b>	0.16
	WanS2V[14]	73.68	642.48	2.20	3.71	4.90	9.02	<b>0.95</b>	0.25
	Ours	64.00	<b>532.52</b>	<b>2.29</b>	<b>3.84</b>	4.64	9.35	<b>0.95</b>	<b>20.88</b>

propriate scripts. For methods that lack support for parallel acceleration, specifically EchoMimic V2 and Ditto, inference is conducted on a single H800 GPU. Regarding resolution, we use a fixed resolution of 720x400 for all models except Hallo3, which does not support arbitrary aspect ratios or resolutions. For Hallo3, we crop both the input and the ground-truth frames to 512x512. Furthermore, EchoMimic is excluded from the long-video comparative experiments, as its reliance on per-frame skeleton templates prevents it from effectively performing long-duration inference.

**Runtime Metrics.** For runtime evaluation, we report two key efficiency metrics. **FPS (Frame Per Second)** is measured from the moment the inference pipeline is initialized and include the full end-to-end cost: the diffusion model’s denoising time, VAE decoding time, and any additional CPU-side processing. **Time-to-First-Frame (TTFF)** accounts for the total latency from audio signal arrival to visual output, calculated as the sum of (i) the random arrival latency—the waiting time between the arrival of an audio interaction signal and the next frame boundary—followed by (ii) the full denoising latency of the first frame and (iii) its VAE decoding cost. Note that random arrival latency depends on the output frame rate, and thus TTFF is inherently coupled with the FPS of the method. All FPS measurements for all methods are evaluated on the GenBench-LongVideo benchmark, where long-sequence testing provides more stable and accurate runtime estimation.

## 11. Algorithm Details.

We provide detailed pseudocode for completeness. As shown in Algorithm 1, our self-forcing DMD training follows [19] but removes the additional forward pass used to refresh the KV cache after denoising. This ensures that the model is consistently trained with noisy KV states, aligning the training process with the actual autoregressive inference process and improving robustness to error accumulation. We refer to this strategy as **History Corrupt**.

Due to the substantial memory footprint of DMD training, we additionally implement a lightweight memory-reduction strategy using **block-wise gradient accumulation** (Algorithm 2). We partition the backward graph by blocks and accumulate the resulting gradients across multiple steps, which preserves training behavior while significantly reducing peak memory usage, enabling even single-node H800 training.

The single-GPU inference procedure is provided in Algorithm 3. It builds upon the rolling-KV-cache inference algorithm from [19] with the addition of AAS and Rolling RoPE, as described in the main text. Figure 6 and Figure 7 provides a visual comparison of the different inference strategies, highlighting key operations such as AAS and Rolling RoPE. The figure also illustrates the rope update performed during autoregressive generation, where the sink frame is continuously re-assigned with updated RoPE.

The multi-GPU TPP inference is detailed in Algorithm 4, which outlines the parallel execution procedure with minimal computation overlap and communication overhead. Figure 8 further visualizes the computation and waiting time of each

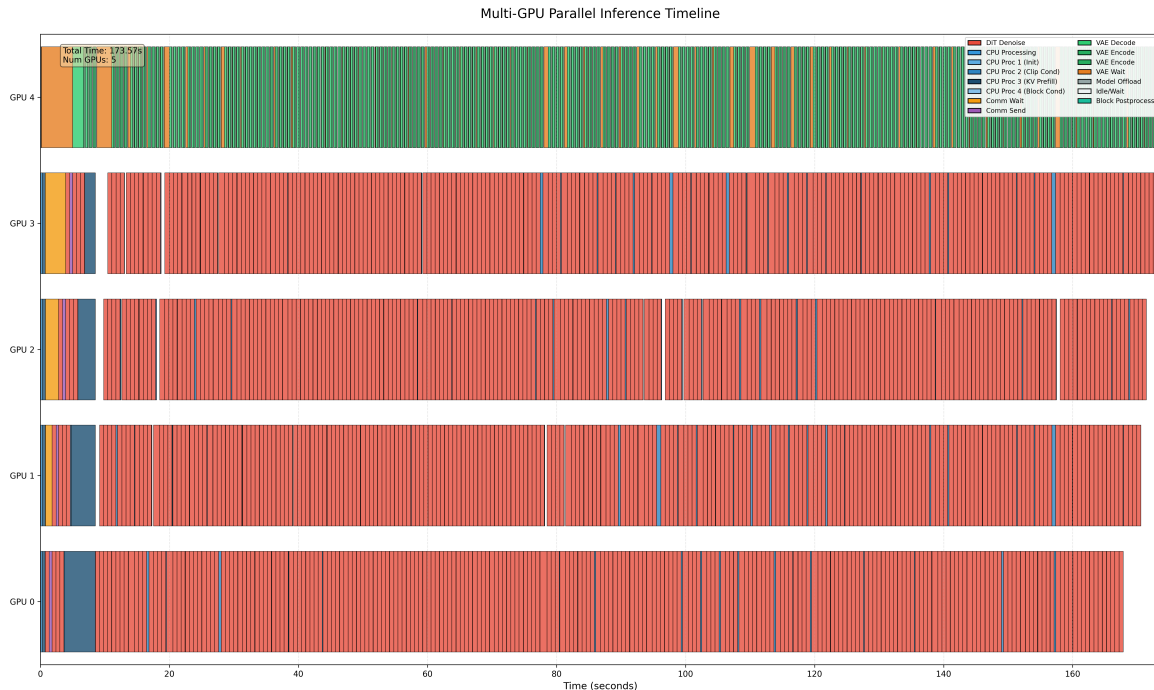


Figure 8. Multi-GPU Parallel Inference Timeline. This chart visualizes the computation and waiting periods for each GPU. The two distinct **white** gaps on the left represent the initial warmup phase (including the secondary warmup for AAS). Following these, the majority of the processing time is dedicated to DiT computation (shown in **red**), reflecting high utilization and stable frame rates. Sporadic **white** gaps (idle time) appearing thereafter are present due to rate fluctuations, but their rarity ensures a negligible impact on performance.

GPU. After the initial warmup (including a second warmup required for AAS), the majority of each GPU’s time is devoted to DIT computation (red), demonstrating high utilization and stable frame rates.

## 12. Additional Visualize results.

We provide additional qualitative examples to further illustrate the model’s long-horizon generation capability. As shown in Figure 9, our method maintains stable identity, consistent lip movements, and coherent visual appearance when extrapolating videos far beyond the training horizon. For three different subjects, the generated frames at 10s, 100s, 1000s, and 10000s remain visually aligned with the reference image and follow the audio-driven motion patterns without exhibiting temporal drift or degradation. These results highlight the robustness of our approach in producing coherent long-duration talking-face videos.

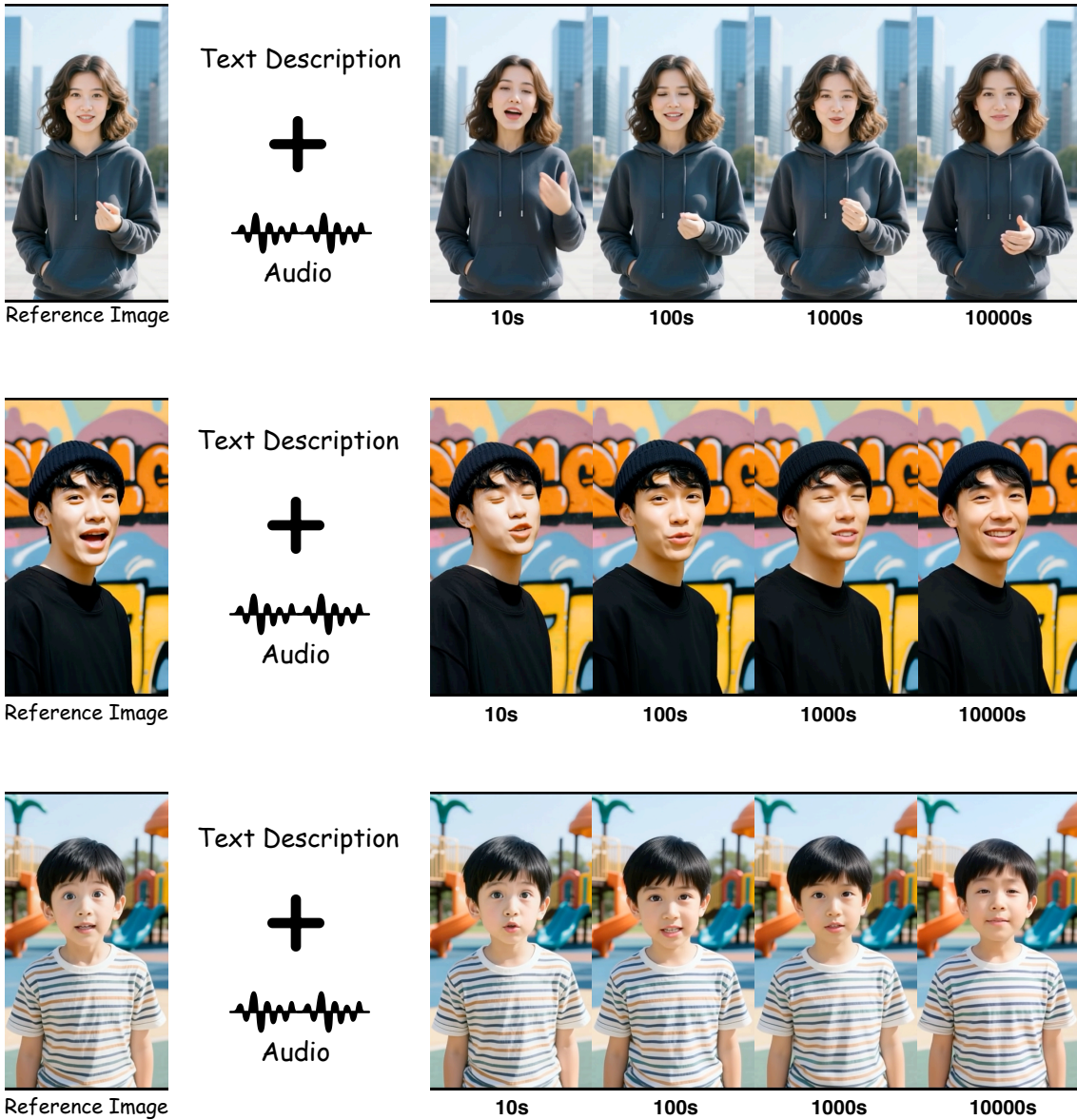


Figure 9. Visualization of the generated video at 10 s, 100 s, 1000 s, and 10000 s, demonstrating the model’s strong capability in long-horizon temporal extrapolation.

---

**Algorithm 1** Self-Forcing DMD with History Corrupt

---

**Require:** Timesteps  $\{t_1, \dots, t_T\}$   
**Require:** Number of video frames  $N$   
**Require:** Conditions of  $N$  frames  $C_{1:N}$  (including audio, text, ref image)  
**Require:** Generator  $G_\theta$  (returns KV embeddings via  $G_\theta^{\text{KV}}$ )

```
1: loop
2:   Initialize model output  $\mathbf{X}_\theta \leftarrow []$ 
3:   Initialize KV cache  $\mathbf{KV} \leftarrow []$ 
4:   Sample  $s \sim \text{Uniform}(1, 2, \dots, T)$ 
5:   for  $i = 1, \dots, N$  do
6:     Initialize  $x_{t_T}^i \sim \mathcal{N}(0, I)$ 
7:     for  $j = T, \dots, s$  do
8:       if  $j = s$  then
9:         Enable gradient computation
10:        Set  $\mathbf{kv}^i, \hat{x}_0^i \leftarrow G_\theta^{\text{KV}}(x_{t_j}^i; t_j, \mathbf{KV}, C_i)$ 
11:         $\mathbf{X}_\theta$ .append( $\hat{x}_0^i$ )
12:        Detach  $\mathbf{kv}^i$  from gradient graph
13:         $\mathbf{KV}$ .append( $\mathbf{kv}^i$ )                                 $\triangleright$  Noisy KV Cache
14:       else
15:         Disable gradient computation
16:         Set  $\hat{x}_0^i \leftarrow G_\theta(x_{t_j}^i; t_j, \mathbf{KV}, C_i)$ 
17:         Sample  $\epsilon \sim \mathcal{N}(0, I)$ 
18:         Set  $x_{t_{j-1}}^i \leftarrow \Psi(\hat{x}_0^i, \epsilon, t_{j-1})$ 
19:       end if
20:     end for
21:   end for
22:   Update  $\theta$  via distribution matching loss
23: end loop
```

---

### 13. Ethical consideration.

Our work focuses on enabling real-time and long-horizon audio-driven avatar generation, which naturally raises concerns related to privacy, consent, and potential misuse. All identity data used in training and evaluation is collected with permission, and our method does not store or reconstruct unauthorized identities. While high-fidelity avatars may be susceptible to impersonation risks, our system is intended solely for legitimate telepresence and interactive applications. We encourage responsible deployment practices such as access control and watermarking to prevent malicious use.

---

**Algorithm 2** Self-Forcing DMD with History Corrupt and Block-wise Gradient Accumulation

---

**Require:** Timesteps  $\{t_1, \dots, t_T\}$   
**Require:** Number of video frames  $N$   
**Require:** Conditions of  $N$  frames  $C_{1:N}$  (including audio, text, ref image)  
**Require:** Generator  $G_\theta$  (extra returns KV embeddings via  $G_\theta^{\text{KV}}$ )

```

1: loop
2:   Initialize model output  $\mathbf{X}_\theta \leftarrow []$ 
3:   Initialize noisy latent cache  $\mathbf{X}_{\text{cache}} \leftarrow []$ 
4:   Initialize KV cache  $\mathbf{KV} \leftarrow []$ 
5:   Sample  $s \sim \text{Uniform}(1, 2, \dots, T)$ 
6:   Disable gradient computation
7:   for  $i = 1, \dots, N$  do
8:     Initialize  $x_{t_T}^i \sim \mathcal{N}(0, I)$ 
9:     for  $j = T, \dots, s$  do
10:       if  $j = s$  then
11:         Set  $\mathbf{kv}^i, \hat{x}_0^i \leftarrow G_\theta^{\text{KV}}(x_{t_j}^i; t_j, \mathbf{KV}, C_i)$ 
12:         Detach  $x_{t_j}^i, \hat{x}_0^i, \mathbf{kv}^i$  from gradient graph
13:          $\mathbf{X}_{\text{cache}}. \text{append}(x_{t_j}^i)$ 
14:          $\mathbf{X}_\theta. \text{append}(\hat{x}_0^i)$ 
15:          $\mathbf{KV}. \text{append}(\mathbf{kv}^i)$ 
16:       else
17:         Set  $\hat{x}_0^i \leftarrow G_\theta(x_{t_j}^i; t_j, \mathbf{KV}, C_i)$ 
18:         Sample  $\epsilon \sim \mathcal{N}(0, I)$ 
19:         Set  $x_{t_{j-1}}^i \leftarrow \Psi(\hat{x}_0^i, \epsilon, t_{j-1})$ 
20:       end if
21:     end for
22:   end for
23:   for  $i = N, \dots, 1$  do
24:     Initialize temporary model output  $\mathbf{X}_i \leftarrow []$ 
25:     for  $j = 1, \dots, N$  do
26:       if  $i = j$  then
27:         Set  $x_{t_s}^i \leftarrow \mathbf{X}_{\text{cache}}[j]$ 
28:         Enable gradient computation
29:         Set  $\hat{x}_0^i \leftarrow G_\theta(x_{t_s}^i; t_s, \mathbf{KV}, C_i)$ 
30:          $\mathbf{X}_i. \text{append}(\hat{x}_0^i)$  ▷ Handle Partial Gradient
31:         Disable gradient computation
32:       else
33:          $\mathbf{X}_i. \text{append}(\mathbf{X}_\theta[j])$ 
34:       end if
35:     end for
36:     Accumulate gradient of  $\theta$  via DMD loss
37:      $\mathbf{KV}. \text{pop}(i)$  ▷ Free Memory
38:   end for
39:   Update  $\theta$ 
40: end loop
  
```

---

---

**Algorithm 3** Single-GPU AR Inference with AAS and Rolling RoPE

---

**Require:** Per-timestep KV caches, each with size  $L$   
**Require:** Timesteps  $\{t_1, \dots, t_T\}$   
**Require:** Number of generated frames  $M$   
**Require:** Conditions of  $N$  frames  $C_{1:N}$  (including audio, text)  
**Require:** Ref image  $R$   
**Require:** Flow-Matching Model  $v_\theta^{\text{KV}}$  (extra returns KV embeddings)  
**Require:** Rolling RoPE transform  $\Phi(\cdot)$   
**Require:** VAE Decoder  $\text{VAE}(\cdot)$

1: Initialize model output  $\mathbf{X}_\theta \leftarrow []$   
2: Initialize KV caches  $\{\mathbf{KV}_1, \dots, \mathbf{KV}_T\} \leftarrow []$   
3: Initialize Rolling Sink Frame  $\mathbf{Sink} \leftarrow R$   
4: Initialize  $dt \leftarrow -1/T$   
5: **for**  $i = 1, \dots, M$  **do**  
6:   Initialize  $x^i \sim \mathcal{N}(0, I)$   
7:   **for**  $j = T, \dots, 1$  **do**  
8:     Set  $\hat{v}_j^i, \mathbf{kv}_j^i \leftarrow v_\theta^{\text{KV}}(x^i; t_j, \mathbf{KV}_j, C_i, \Phi(\mathbf{Sink}))$  ▷ RoPE Update  
9:     Set  $x^i \leftarrow x^i + \hat{v}_j^i dt$   
10:    **if**  $|\mathbf{KV}_j| = L$  **then**  
11:      $\mathbf{KV}_j.\text{pop}(0)$   
12:    **end if**  
13:      $\mathbf{KV}_j.\text{append}(\mathbf{kv}_j^i)$   
14:    **end for**  
15:     $\mathbf{X}_\theta.\text{append}(\text{VAE}(x^i))$   
16:    **if**  $i = 1$  **then**  
17:        $\mathbf{Sink} \leftarrow x^i$  ▷ AAS Update  
18:    **end if**  
19: **end for**  
20: **return**  $\mathbf{X}_\theta$

---

---

**Algorithm 4** TPP with AAS and Rolling RoPE

---

**Require:** GPU Index  $k$   
**Require:** Per-timestep KV caches, each with size  $L$   
**Require:** Timesteps  $\{t_1, \dots, t_T\}$   
**Require:** Number of generated frames  $M$   
**Require:** Conditions of  $N$  frames  $C_{1:N}$  (including audio, text)  
**Require:** Ref image  $R$   
**Require:** Flow-Matching Model  $v_\theta^{\text{KV}}$  (extra returns KV embeddings)  
**Require:** Rolling RoPE transform  $\Phi(\cdot)$   
**Require:** VAE Decoder  $\text{VAE}(\cdot)$

1: Initialize model output  $\mathbf{X}_\theta \leftarrow []$   
 2: Initialize KV cache  $\mathbf{KV} \leftarrow []$   
 3: Initialize Rolling Sink Frame  $\mathbf{Sink} \leftarrow R$   
 4: Initialize  $dt \leftarrow -1/T$   
 5: **for**  $i = 1, \dots, M$  **do**  
 6:   **if**  $k=1$  **then**  
 7:     Initialize  $x^i \sim \mathcal{N}(0, I)$   
 8:   **else**  
 9:      $x^i \leftarrow \text{dist.recv}()$   
 10:   **end if**  
 11:   **if**  $k=T+1$  **then** ▷ VAE Device  
 12:      $\mathbf{X}_\theta . \text{append}(\text{VAE}(x^i))$   
 13:     **if**  $i = 1$  **then**  
 14:        $\mathbf{Sink} \leftarrow \mathbf{X}_\theta[i]$   
 15:        $\text{dist.broadcast}(\mathbf{Sink})$  ▷ Broadcast AAS  
 16:     **end if**  
 17:     **continue**  
 18:   **else** ▷ DiT Device  
 19:     **if**  $i=2$  **then**  
 20:        $\mathbf{Sink} \leftarrow \text{dist.recv}()$  ▷ Update AAS  
 21:     **end if**  
 22:     Set  $\hat{v}_k^i, \mathbf{kv}^i \leftarrow v_\theta^{\text{KV}}(x^i; t_{T-k+1}, \mathbf{KV}, C_i, \Phi(\mathbf{Sink}))$   
 23:     **if**  $|\mathbf{KV}| = L$  **then**  
 24:        $\mathbf{KV}.\text{pop}(0)$   
 25:     **end if**  
 26:      $\mathbf{KV}.\text{append}(\mathbf{kv}^i)$   
 27:     Set  $x^i \leftarrow x^i + \hat{v}_k^i dt$   
 28:      $\text{dist.send}(x^i)$   
 29:   **end if**  
 30: **end for**  
 31: **return**  $\mathbf{X}_\theta$ 


---

## References

- [1] Tenglong Ao. Body of her: A preliminary study on end-to-end humanoid agent. *arXiv preprint arXiv:2408.02879*, 2024. 3
- [2] Tim Brooks, Bill Peebles, Connor Holmes, Will DePue, Yufei Guo, Li Jing, David Schnurr, Joe Taylor, Troy Luhman, Eric Luhman, Clarence Ng, Ricky Wang, and Aditya Ramesh. Video generation models as world simulators. 2024. 2, 3
- [3] Boyuan Chen, Diego Martí Monsó, Yilun Du, Max Simchowitz, Russ Tedrake, and Vincent Sitzmann. Diffusion forcing: Next-token prediction meets full-sequence diffusion. *Advances in Neural Information Processing Systems*, 37:24081–24125, 2024. 2
- [4] Ming Chen, Liyuan Cui, Wenyuan Zhang, Haoxian Zhang, Yan Zhou, Xiaohan Li, Songlin Tang, Jiwen Liu, Borui Liao, Hejia Chen, et al. Midas: Multimodal interactive digital-human synthesis via real-time autoregressive video generation. *arXiv preprint arXiv:2508.19320*, 2025. 3
- [5] Joon Son Chung and Andrew Zisserman. Out of time: automated lip sync in the wild. In *Computer Vision–ACCV 2016 Workshops: ACCV 2016 International Workshops, Taipei, Taiwan, November 20–24, 2016, Revised Selected Papers, Part II 13*, pages 251–263. Springer, 2017. 7
- [6] Jiahao Cui, Hui Li, Yun Zhan, Hanlin Shang, Kaihui Cheng, Yuqi Ma, Shan Mu, Hang Zhou, Jingdong Wang, and Siyu Zhu. Hallo3: Highly dynamic and realistic portrait image animation with video diffusion transformer. In *Proceedings of the Computer Vision and Pattern Recognition Conference*, pages 21086–21095, 2025. 2, 7, 9, 4
- [7] Justin Cui, Jie Wu, Ming Li, Tao Yang, Xiaojie Li, Rui Wang, Andrew Bai, Yuanhao Ban, and Cho-Jui Hsieh. Self-forcing++: Towards minute-scale high-quality video generation. *arXiv preprint arXiv:2510.02283*, 2025. 2, 3
- [8] Fangyu Du, Taiqing Li, Ziwei Zhang, Qian Qiao, Tan Yu, Dingcheng Zhen, Xu Jia, Yang Yang, Shunshun Yin, and Siyuan Liu. Rap: Real-time audio-driven portrait animation with video diffusion transformer. *arXiv preprint arXiv:2508.05115*, 2025. 3
- [9] Zhihao Du, Yuxuan Wang, Qian Chen, Xian Shi, Xiang Lv, Tianyu Zhao, Zhifu Gao, Yexin Yang, Changfeng Gao, Hui Wang, Fan Yu, Huadai Liu, Zhengyan Sheng, Yue Gu, Chong Deng, Wen Wang, Shiliang Zhang, Zhijie Yan, and Jingren Zhou. Cosyvoice 2: Scalable streaming speech synthesis with large language models, 2024. 6
- [10] Ariel Ephrat, Inbar Mosseri, Oran Lang, Tali Dekel, Kevin Wilson, Avinatan Hassidim, William T Freeman, and Michael Rubinstein. Looking to listen at the cocktail party: A speaker-independent audio-visual model for speech separation. *arXiv preprint arXiv:1804.03619*, 2018. 6
- [11] Xiangyu Fan, Zesong Qiu, Zhuguanyu Wu, Fanzhou Wang, Zhiqian Lin, Tianxiang Ren, Dahua Lin, Ruihao Gong, and Lei Yang. Phased dmd: Few-step distribution matching distillation via score matching within subintervals. *arXiv preprint arXiv:2510.27684*, 2025. 7
- [12] Kevin Frans, Danijar Hafner, Sergey Levine, and Pieter Abbeel. One step diffusion via shortcut models. *arXiv preprint arXiv:2410.12557*, 2024. 3
- [13] Qijun Gan, Ruizi Yang, Jianke Zhu, Shaofei Xue, and Steven Hoi. Omniaavatar: Efficient audio-driven avatar video generation with adaptive body animation. *arXiv preprint arXiv:2506.18866*, 2025. 2, 6, 7, 9, 4
- [14] Xin Gao, Li Hu, Siqi Hu, Mingyang Huang, Chaonan Ji, Dechao Meng, Jinwei Qi, Pengchong Qiao, Zhen Shen, Yafei Song, Ke Sun, Linrui Tian, Guangyuan Wang, Qi Wang, Zhongjian Wang, Jiayu Xiao, Sheng Xu, Bang Zhang, Peng Zhang, Xindi Zhang, Zhe Zhang, Jingren Zhou, and Lian Zhuo. Wan-s2v: Audio-driven cinematic video generation, 2025. 2, 7, 9, 4
- [15] Xin Gao, Li Hu, Siqi Hu, Mingyang Huang, Chaonan Ji, Dechao Meng, Jinwei Qi, Pengchong Qiao, Zhen Shen, Yafei Song, et al. Wan-s2v: Audio-driven cinematic video generation. *arXiv preprint arXiv:2508.18621*, 2025. 2, 6
- [16] Ying Guo, Xi Liu, Cheng Zhen, Pengfei Yan, and Xiaoming Wei. Arig: Autoregressive interactive head generation for real-time conversations. *arXiv preprint arXiv:2507.00472*, 2025. 3
- [17] Yoav HaCohen, Nisan Chiprut, Benny Brazowski, Daniel Shalem, Dudu Moshe, Eitan Richardson, Eran Levin, Guy Shiran, Nir Zabari, Ori Gordon, et al. Ltx-video: Realtime video latent diffusion. *arXiv preprint arXiv:2501.00103*, 2024. 2, 3
- [18] Martin Heusel, Hubert Ramsauer, Thomas Unterthiner, Bernhard Nessler, and Sepp Hochreiter. Gans trained by a two time-scale update rule converge to a local nash equilibrium. *Advances in neural information processing systems*, 30, 2017. 7
- [19] Xun Huang, Zhengqi Li, Guande He, Mingyuan Zhou, and Eli Shechtman. Self forcing: Bridging the train-test gap in autoregressive video diffusion. *arXiv preprint arXiv:2506.08009*, 2025. 2, 3, 5, 6, 1
- [20] Jianwen Jiang, Weihong Zeng, Zerong Zheng, Jiaqi Yang, Chao Liang, Wang Liao, Han Liang, Yuan Zhang, and Mingyuan Gao. Omnihuman-1.5: Instilling an active mind in avatars via cognitive simulation. *arXiv preprint arXiv:2508.19209*, 2025. 2
- [21] Akio Kodaira, Tingbo Hou, Ji Hou, Masayoshi Tomizuka, and Yue Zhao. Streamdit: Real-time streaming text-to-video generation. *arXiv preprint arXiv:2507.03745*, 2025. 2
- [22] Weijie Kong, Qi Tian, Zijian Zhang, Rox Min, Zuozhuo Dai, Jin Zhou, Jiangfeng Xiong, Xin Li, Bo Wu, Jianwei Zhang, et al. Hunyuvideo: A systematic framework for large video generative models. *arXiv preprint arXiv:2412.03603*, 2024. 3
- [23] Tianhong Li, Yonglong Tian, He Li, Mingyang Deng, and Kaiming He. Autoregressive image generation without vector quantization. *Advances in Neural Information Processing Systems*, 37:56424–56445, 2024. 3
- [24] Tianqi Li, Ruobing Zheng, Minghui Yang, Jingdong Chen, and Ming Yang. Ditto: Motion-space diffusion for controllable realtime talking head synthesis. *arXiv preprint arXiv:2411.19509*, 2024. 2, 3, 7, 9, 4

- [25] Yaron Lipman, Ricky TQ Chen, Heli Ben-Hamu, Maximilian Nickel, and Matt Le. Flow matching for generative modeling. *arXiv preprint arXiv:2210.02747*, 2022. 3
- [26] Kunhao Liu, Wenbo Hu, Jiale Xu, Ying Shan, and Shijian Lu. Rolling forcing: Autoregressive long video diffusion in real time. *arXiv preprint arXiv:2509.25161*, 2025. 2
- [27] Chetwin Low and Weimin Wang. Talkingmachines: Real-time audio-driven facetime-style video via autoregressive diffusion models. *arXiv preprint arXiv:2506.03099*, 2025. 3, 5, 6
- [28] Cheng Lu and Yang Song. Simplifying, stabilizing and scaling continuous-time consistency models. *arXiv preprint arXiv:2410.11081*, 2024. 3
- [29] Weijian Luo. Diff-instruct++: Training one-step text-to-image generator model to align with human preferences. *arXiv preprint arXiv:2410.18881*, 2024. 3, 7
- [30] Weijian Luo, Tianyang Hu, Shifeng Zhang, Jiacheng Sun, Zhenguo Li, and Zhihua Zhang. Diff-instruct: A universal approach for transferring knowledge from pre-trained diffusion models. *Advances in Neural Information Processing Systems*, 36:76525–76546, 2023. 3
- [31] Yihong Luo, Tianyang Hu, Jiacheng Sun, Yujun Cai, and Jing Tang. Learning few-step diffusion models by trajectory distribution matching. *arXiv preprint arXiv:2503.06674*, 2025. 3, 7
- [32] Dechao Meng, Steven Xiao, Xindi Zhang, Guangyuan Wang, Peng Zhang, Qi Wang, Bang Zhang, and Liefeng Bo. Mirrorme: Towards realtime and high fidelity audio-driven halfbody animation. *arXiv preprint arXiv:2506.22065*, 2025. 3
- [33] Rang Meng, Xingyu Zhang, Yuming Li, and Chenguang Ma. Echomimicv2: Towards striking, simplified, and semi-body human animation, 2025. 7, 9, 4
- [34] KR Prajwal, Rudrabha Mukhopadhyay, Vinay P Namboodiri, and CV Jawahar. A lip sync expert is all you need for speech to lip generation in the wild. In *Proceedings of the 28th ACM international conference on multimedia*, pages 484–492, 2020. 3
- [35] Nabyl Quignon, Baptiste Chopin, Yaohui Wang, and Antitza Dantcheva. Theval. evaluation framework for talking head video generation, 2025. 8
- [36] Yang Song, Prafulla Dhariwal, Mark Chen, and Ilya Sutskever. Consistency models. 2023. 3
- [37] Linrui Tian, Qi Wang, Bang Zhang, and Liefeng Bo. Emo: Emote portrait alive generating expressive portrait videos with audio2video diffusion model under weak conditions. In *European Conference on Computer Vision*, pages 244–260. Springer, 2024. 3
- [38] Shuyuan Tu, Yueming Pan, Yinming Huang, Xintong Han, Zhen Xing, Qi Dai, Chong Luo, Zuxuan Wu, and Yu-Gang Jiang. Stableavatar: Infinite-length audio-driven avatar video generation. *arXiv preprint arXiv:2508.08248*, 2025. 2, 6, 7, 9, 4
- [39] Thomas Unterthiner, Sjoerd Van Steenkiste, Karol Kurach, Raphael Marinier, Marcin Michalski, and Sylvain Gelly. Towards accurate generative models of video: A new metric & challenges. *arXiv preprint arXiv:1812.01717*, 2018. 7
- [40] Team Wan, Ang Wang, Baole Ai, Bin Wen, Chaojie Mao, Chen-Wei Xie, Di Chen, Fei Yu, Haiming Zhao, Jianxiao Yang, et al. Wan: Open and advanced large-scale video generative models. *arXiv preprint arXiv:2503.20314*, 2025. 2, 3
- [41] Mengchao Wang, Qiang Wang, Fan Jiang, Yaqi Fan, Yunpeng Zhang, Yonggang Qi, Kun Zhao, and Mu Xu. Fantasytalking: Realistic talking portrait generation via coherent motion synthesis. In *Proceedings of the 33rd ACM International Conference on Multimedia*, pages 9891–9900, 2025. 8
- [42] Zhongjian Wang, Peng Zhang, Jinwei Qi, Guangyuan Wang, Sheng Xu, Bang Zhang, and Liefeng Bo. Omnitalker: Real-time text-driven talking head generation with in-context audio-visual style replication. *arXiv e-prints*, pages arXiv–2504, 2025. 3
- [43] Chenfei Wu, Jiahao Li, Jingren Zhou, Junyang Lin, Kaiyuan Gao, Kun Yan, Sheng ming Yin, Shuai Bai, Xiao Xu, Yilei Chen, Yuxiang Chen, Zecheng Tang, Zekai Zhang, Zhengyi Wang, An Yang, Bowen Yu, Chen Cheng, Dayiheng Liu, Deqing Li, Hang Zhang, Hao Meng, Hu Wei, Jingyuan Ni, Kai Chen, Kuan Cao, Liang Peng, Lin Qu, Minggang Wu, Peng Wang, Shuting Yu, Tingkun Wen, Wensen Feng, Xiaoxiao Xu, Yi Wang, Yichang Zhang, Yongqiang Zhu, Yujia Wu, Yuxuan Cai, and Zenan Liu. Qwen-image technical report, 2025. 6
- [44] Haoning Wu, Zicheng Zhang, Weixia Zhang, Chaofeng Chen, Liang Liao, Chunyi Li, Yixuan Gao, Annan Wang, Erli Zhang, Wenxiu Sun, et al. Q-align: Teaching lmms for visual scoring via discrete text-defined levels. *arXiv preprint arXiv:2312.17090*, 2023. 7
- [45] You Xie, Tianpei Gu, Zenan Li, Chenxu Zhang, Guoxian Song, Xiaochen Zhao, Chao Liang, Jianwen Jiang, Hongyi Xu, and Linjie Luo. X-streamer: Unified human world modeling with audiovisual interaction. *arXiv preprint arXiv:2509.21574*, 2025. 3, 4
- [46] Shuai Yang, Wei Huang, Ruihang Chu, Yicheng Xiao, Yuyang Zhao, Xianbang Wang, Muyang Li, Enze Xie, Yingcong Chen, Yao Lu, et al. Longlive: Real-time interactive long video generation. *arXiv preprint arXiv:2509.22622*, 2025. 2, 3, 5, 1
- [47] Shaoshu Yang, Zhe Kong, Feng Gao, Meng Cheng, Xiangyu Liu, Yong Zhang, Zhuoliang Kang, Wenhan Luo, Xunliang Cai, Ran He, et al. Infinitetalk: Audio-driven video generation for sparse-frame video dubbing. *arXiv preprint arXiv:2508.14033*, 2025. 2
- [48] Tianwei Yin, Michaël Gharbi, Taesung Park, Richard Zhang, Eli Shechtman, Fredo Durand, and Bill Freeman. Improved distribution matching distillation for fast image synthesis. *Advances in neural information processing systems*, 37:47455–47487, 2024. 3, 4
- [49] Tianwei Yin, Michaël Gharbi, Richard Zhang, Eli Shechtman, Fredo Durand, William T Freeman, and Taesung Park. One-step diffusion with distribution matching distillation. In *Proceedings of the IEEE/CVF conference on computer vision and pattern recognition*, pages 6613–6623, 2024. 3

- [50] Tianwei Yin, Qiang Zhang, Richard Zhang, William T Freeman, Fredo Durand, Eli Shechtman, and Xun Huang. From slow bidirectional to fast autoregressive video diffusion models. In *Proceedings of the Computer Vision and Pattern Recognition Conference*, pages 22963–22974, 2025. [2](#), [3](#), [4](#), [5](#), [1](#)
- [51] Haojie Yu, Zhaonian Wang, Yihan Pan, Meng Cheng, Hao Yang, Chao Wang, Tao Xie, Xiaoming Xu, Xiaoming Wei, and Xunliang Cai. Llia-enabling low-latency interactive avatars: Real-time audio-driven portrait video generation with diffusion models. *arXiv preprint arXiv:2506.05806*, 2025. [3](#)
- [52] Wenxuan Zhang, Xiaodong Cun, Xuan Wang, Yong Zhang, Xi Shen, Yu Guo, Ying Shan, and Fei Wang. Sadtalker: Learning realistic 3d motion coefficients for stylized audio-driven single image talking face animation. In *Proceedings of the IEEE/CVF conference on computer vision and pattern recognition*, pages 8652–8661, 2023. [3](#)
- [53] Dingcheng Zhen, Shunshun Yin, Shiyang Qin, Hou Yi, Ziwei Zhang, Siyuan Liu, Gan Qi, and Ming Tao. Teller: Real-time streaming audio-driven portrait animation with autoregressive motion generation. In *Proceedings of the Computer Vision and Pattern Recognition Conference*, pages 21075–21085, 2025. [3](#)
- [54] Kaiwen Zheng, Yuji Wang, Qianli Ma, Huayu Chen, Jintao Zhang, Yogesh Balaji, Jianfei Chen, Ming-Yu Liu, Jun Zhu, and Qinsheng Zhang. Large scale diffusion distillation via score-regularized continuous-time consistency. *arXiv preprint arXiv:2510.08431*, 2025. [3](#)
- [55] Yongming Zhu, Longhao Zhang, Zhengkun Rong, Tianshu Hu, Shuang Liang, and Zhipeng Ge. Infp: Audio-driven interactive head generation in dyadic conversations. In *Proceedings of the Computer Vision and Pattern Recognition Conference*, pages 10667–10677, 2025. [3](#)